Direct observation of dipolar chains in ferrofluids in zero field using cryogenic electron microscopy

2003 J. Phys.: Condens. Matter 15 S1451

(http://iopscience.iop.org/0953-8984/15/15/310)

INSTITUTE OF PHYSICS PUBLISHING JOURNAL OF PHYSICS: CONDENSED MATTER

J. Phys.: Condens. Matter **15** (2003) S1451–S1470 PII: S0953-8984(03)54823-8

Direct observation of dipolar chains in ferrofluids in zero field using cryogenic electron microscopy

K Butter[1], P H Bomans[2], P M Frederik[2], G J Vroege[1] and A P Philipse[1,3]

[1] Van 't Hoff Laboratory for Physical and Colloid Chemistry, Debye Institute, Utrecht University, Padualaan 8, 3584 CH Utrecht, The Netherlands
[2] EM Unit, Department of Pathology, University of Maastricht, Universiteitssingel 50, 6229 ER Maastricht, The Netherlands

E-mail: a.p.philipse@chem.uu.nl

Received 16 October 2002
Published 7 April 2003
Online at stacks.iop.org/JPhysCM/15/S1451

Abstract

The particle structure of ferrofluids is studied *in situ*, by cryogenic electron microscopy, on vitrified films of iron and magnetite dispersions. By means of synthesis of iron colloids with controlled particle size and different types of surfactant, dipolar particle interactions can be varied over a broad range, which significantly influences the ferrofluid particle structure. Our experiments on iron dispersions (in contrast to magnetite dispersions) for the first time demonstrate, in ferrofluids in zero field, a transition with increasing particle size from separate particles to linear chains of particles (Butter K, Bomans P H, Frederik P M, Vroege G J and Philipse A P 2003 *Nature Mater.* **2** 88). These chains, already predicted theoretically by de Gennes and Pincus (de Gennes P G and Pincus P A 1970 *Phys. Kondens. Mater.* **11** 189), very much resemble the fluctuating chains found in simulations of dipolar fluids (Weis J J 1998 *Mol. Phys.* **93** 361, Chantrell R W, Bradbury A, Popplewell J and Charles S W 1982 *J. Appl. Phys.* **53** 2742). Decreasing the range of steric repulsion between particles by employing a thinner surfactant layer is found to change particle structures as well. The dipolar nature of the aggregation is confirmed by the alignment of existing chains and individual particles in the field direction upon vitrification of dispersions in a saturating magnetic field. Frequency-dependent susceptibility measurements indicate that particle structures in truly three-dimensional ferrofluids are qualitatively similar to those in liquid films.

1. Introduction

Ferrofluids (dispersions of magnetic colloids) behave as magnetizable liquids (figure 1) and are applied e.g. as rotary shaft seals [5] or magnetic carriers for drugs [6]. In addition, ferrofluids

[3] Author to whom any correspondence should be addressed.

Figure 1. An example of an iron dispersion, synthesized by thermal decomposition of $Fe(CO)_5$ in decalin in the presence of modified PIB following [18] and always stored under nitrogen atmosphere. Average particle radii were varied by changing the $Fe(CO)_5$/PIB ratio. The dispersion exhibits the equilibrium shape in a field gradient typical for a stable ferrofluid [16].

are of interest as a model system for dipolar fluids in general, since they consist of freely rotating permanent dipoles in a non-magnetic matrix, which can be studied relatively easily because of their large size in comparison to molecular dipoles. How dipole–dipole interactions influence particle structure and phase behaviour in ferrofluids is a fascinating question, which has been a subject of research for decades already [2, 7, 8]. In 1970, de Gennes and Pincus [2] predicted a van der Waals-like phase diagram and the presence of chain-like structures in ferrofluids in zero field. Since then, many theories [9, 10] and simulations [3, 11] have been published relating to the subject, which remains a matter of debate [7, 8]. Despite various studies [12–15], direct experimental proof for the existence of particle chains is lacking. Conclusive evidence is difficult to obtain from indirect techniques; e.g. scattering patterns from ferrofluids in zero field are isotropic and extracting the shape and distribution of aggregates, if any, from measured intensity profiles is far from straightforward. Using conventional transmission electron microscopy (TEM), original particle structures may be severely distorted due to drying effects, giving no direct information about particle arrangement in the fluid state. In addition, most commonly studied ferrofluids consist of magnetite particles (Fe_3O_4), where dipole–dipole interactions are relatively weak [8, 16], making it questionable whether significant chain formation in zero field occurs in these dispersions anyway.

Cryogenic transmission electron microscopy (cryo-TEM) images of vitrified liquid films were obtained via low-dose TEM. A fast temperature quench of films of dispersions vitrifies the solvent, arresting thermal diffusion of colloids on the timescale of vitrification. This enables one to study particle structures in a ferrofluid *in situ*. Because dipole–dipole interactions are very sensitive to particle dipole moments and interparticle distances, ferrofluid microstructures are expected to be influenced significantly by particle radii, particle concentrations and the thickness of their surfactant layer. We therefore synthesized iron dispersions for our study, following a method by which particle sizes can be controlled over a broad size range (with a narrow size distribution) and, in addition, particles can be stabilized by different

surfactants [17, 18]. These dispersions were studied by cryo-TEM to systematically investigate particle structures in ferrofluids for two different surfactant layers as a function of particle size. In addition, we studied conventional oleic-acid-coated magnetite dispersions. To verify the dominance of dipolar forces in our dispersions, some iron samples were also vitrified in a saturating magnetic field. Because cryo-TEM studies thin films of dispersions, which should be considered as quasi-two-dimensional, particle structures of the same dispersions in the bulk were studied by frequency-dependent susceptibility measurements for comparison. This paper is organized as follows: in section 2 the theory and equations relevant for the various measuring techniques are explained. Section 3 describes the experimental methods of the synthesis and characterization of our ferrofluids, as well as of the cryo-electron microscopy and susceptibility measurements. Results are presented and discussed in section 4.

2. Theoretical background

2.1. Ferrofluids

Ferrofluids consist of monodomain magnetic colloids, which can be considered as point dipoles with a magnetic moment $\mu = (4\pi/3)a_M^3 m_s$, a_M being the particle radius of the magnetic core and m_s the saturation magnetization of the particle material (1.7×10^6 and 0.48×10^6 A m^{-1} for bulk iron and magnetite respectively [16]). In a dispersion in zero field, all magnetic moments are oriented randomly due to thermal motion of particles and the net magnetic moment of the sample M is zero. A magnetic field aligns particle dipoles in the field direction, inducing a magnetic moment in the sample. For dilute ferrofluids, M as a function of the magnetic field strength H is given by the Langevin equation [16]:

$$M(H) = M_s\left(\coth\left(\frac{\mu_0\mu H}{kT}\right) - \frac{kT}{\mu_0\mu H}\right) \tag{1}$$

where M_s is the saturation magnetization of the sample, reached upon complete alignment of all particles in the field direction. For low fields, equation (1) can be approximated by

$$M(H) \approx M_s\left(\frac{\mu_0\mu H}{3kT}\right) \qquad (\text{for } \mu_0\mu H \ll kT). \tag{2}$$

M_s and the initial susceptibility $\chi_i = (\partial M/\partial H)_{H=0}$ can be determined experimentally from the magnetization curve, from which the mean magnetic particle radius a_M (assuming a spherical shape) is calculated, using

$$a_M^3 = \frac{\chi_i}{M_s}\left(\frac{9\,kT}{4\pi\,\mu_0 m_s}\right). \tag{3}$$

Note that this radius only includes the magnetic part of the particle, which will be somewhat smaller than the physical particle radius, if particles contain a non-magnetic surface layer [16]. The magnetic interaction potential between two dipoles μ_i and μ_j depends on their magnitude and orientation and is given by

$$U_{d-d} = \frac{\mu_0}{4\pi}\left(\frac{\vec{\mu}_i \cdot \vec{\mu}_j}{r^3} - \frac{3(\vec{\mu}_i \cdot \vec{r})(\vec{\mu}_j \cdot \vec{r})}{r^5}\right) \tag{4}$$

where $\vec{r}$ connects the two dipoles. The attraction is maximal when particle dipoles are oriented head to tail and for monodisperse particles it is equal to

$$U_{max} = -2\frac{\mu_0}{4\pi}\left(\frac{\mu^2}{r^3}\right) \qquad \left(\mu = \tfrac{4}{3}\pi a_M^3 m_s\right). \tag{5}$$

Note that U_{max} is proportional to a_M^6/σ^3 when particles are at the closest centre-to-centre distance $r = \sigma$. The surfactant layers of sterically stabilized particles, often modelled as hard spheres, cause a strong repulsive potential U_{rep}, where $U_{rep} = 0$ for $r > \sigma$ and $U_{rep} = \infty$ for $r \leqslant \sigma$. Here, the minimal interparticle distance is determined by their effective hard-sphere diameter σ, consisting of twice the sum of the core radius a_{core} and the thickness of the surfactant layers t_s. A third contribution to the interaction potential between particles is the van der Waals attraction, given by the Hamaker formula for the London–van der Waals attractive interaction energy between spherical particles:

$$V_{vdW} = -\frac{A}{6}\left[\frac{2a_{core}^2}{r^2 - 4a_{core}^2} + \frac{2a_{core}^2}{r^2} + \ln\left(1 - \frac{4a_{core}^2}{r^2}\right)\right] \tag{6}$$

with A the Hamaker constant ($A \approx 10^{-19}$ J for iron and iron oxide [16]). For magnetic colloids, V_{vdW} is of the order of kT. Except for the fact that the van der Waals interaction is isotropic, whereas the magnetic interaction is anisotropic, another important difference is that the former is a function of a_{core}/r only, whereas the latter has a stronger particle volume dependence [19]. Thus, on increasing the particle size, the magnetic attraction will become relatively more important; for example, the magnetic attraction is estimated to be dominant for oleic-acid-coated maghemite particle radii larger than about 5 nm [19], while for smaller particles the van der Waals attraction is more important.

As the strength of the dipole–dipole interaction scales with a_M^6 (see equation (5)) and is inversely proportional to r^3, the ferrofluid microstructure is expected to be very sensitive to particle radii as well as the surfactant layer thickness. For a collection of dipoles, it is energetically favourable to form linear chains of dipoles. For example, the energy gain U_{d-c} for adding one dipole to the end of an infinitely long chain is [20]

$$U_{d-c} = U_{max}\sum_{n=1}^{\infty}\frac{1}{n^3} \approx 1.202\,U_{max}. \tag{7}$$

The attraction potential between two long chains of dipoles oriented head to tail at closest contact is even larger (approximately $1.64\,U_{max}$) [21].

The interaction potential between two chains of dipoles in the lateral direction (perpendicular to the chain axes) is analogous to the case of chains of particles in electrorheological fluids calculated by Halsey and Toor [22, 23]. They found that the dominant interaction between two parallel chains of dipoles in a saturating magnetic field (for $l \gg a$, with dipole spacing $2a$ at lateral distance l) is induced by fluctuations in their shape and has the same form as the van der Waals attraction between chains (which scales with l^{-5}) [23]. Although for electrorheological fluids the fluctuation-induced dipolar interaction between parallel chains is an order of magnitude larger than the van der Waals interaction, for ferrofluids they are of the same order due to the high Hamaker constants of iron and iron oxide. Still, the effect of the fluctuation coupling can be seen as an increase of the Hamaker constant. Only at small distance (of the order of a particle diameter) is the interaction potential between parallel chains determined by the discrete nature of the particle chain and this is attractive when chains are shifted half a particle diameter with respect to each other [23].

2.2. Small-angle x-ray scattering

The average scattered intensity $I(q)$ of a suspension of identical spherical colloidal particles with number concentration c_p, particle volume V_p and electron density difference from the solvent $\Delta\rho$ is given by [24]

$$I(q) \propto c_p(\Delta\rho)^2 V_p^2 P(q) S(q). \tag{8}$$

Here, q is the magnitude of the momentum transfer vector, $P(q)$ the form factor and $S(q)$ the structure factor. For scattering curves of dilute suspensions the radius of gyration R_g can be obtained from the Guinier approximation for $q < 2/R_g$ [24]:

$$I(q) = I(q = 0)\exp(-q^2R_g^2/3). \tag{9}$$

For homogeneous spheres, the radius of gyration is related to the sphere radius R by

$$R_g^2 = 3R^2/5. \tag{10}$$

For polydisperse systems, the average particle radius as determined from the Guinier plot is an overestimation. For size distributions with a small standard deviation s, the apparent radius derived from the scattering at low q can be corrected for polydispersity, according to [24]

$$R = \langle R\rangle\left[1 + \frac{13}{2}\left(\frac{s}{\langle R\rangle}\right)^2\right]. \tag{11}$$

Here, R is the apparent and $\langle R\rangle$ is the number-average particle radius. Dividing the scattered intensities of a dispersion at a given volume fraction by those of a dilute dispersion gives the experimental static structure factor. The peak in the structure factor roughly corresponds to the distance of nearest approach between particles, given by Bragg's law:

$$d_c q_{max} = 2\pi. \tag{12}$$

Here, q_{max} is the q-value at the maximum intensity and d_c is the centre-to-centre distance of nearest approach.

2.3. Susceptibility as a function of frequency

The frequency-dependent susceptibility of a ferrofluid can be measured using two concentric coils (having N loops) with length L much smaller than the coil radius R. An AC $I(\omega) = I_{ampl}\exp(\mathrm{i}\omega t)$ generates an external AC magnetic field $H(\omega)$ at the centre of such a coil [25]:

$$H(\omega) = NI(\omega)/2R. \tag{13}$$

The magnetic induction $B(\omega)$ differs from $\mu_0 H(\omega)$ when a magnetic sample with susceptibility $\chi(\omega)$ is placed inside the coil [25]:

$$B(\omega) = \mu_0 H(\omega)(1 + \chi(\omega)). \tag{14}$$

Using two concentric coils (with N_1 and N_2 loops), with $I(\omega)$ flowing through the primary (outer) coil with radius R_1, $H(\omega)$ induces an AC voltage $V(\omega)$ in the secondary coil equal to $-\partial\phi/\partial t$ where $\phi = N_2 B(\omega)A$ with A the area of the coil [25]. This means that the susceptibility of a sample can be determined by measuring the induced voltage $V(\omega)$ in the secondary coil:

$$V(\omega) = -\mathrm{i}\omega A(1 + \chi(\omega))N_2(\mu_0 N_1/2R_1)I_{ampl}\exp(\mathrm{i}\omega t). \tag{15}$$

The complex relative magnetic susceptibility of a ferrofluid in low fields is given by [26]

$$\chi(\omega) = \chi'(\omega) - \mathrm{i}\chi''(\omega). \tag{16}$$

When a single relaxation time τ is involved, $\chi(\omega)$ is given by [27]

$$\chi(\omega) = \chi_\infty + (\chi_0 - \chi_\infty)/(1 + \mathrm{i}\omega\tau) \tag{17}$$

where χ_0 and χ_∞ are the magnetic susceptibilities in the low- and the high-frequency limit respectively. The mobility of magnetic moments in a ferrofluid is determined by two relaxation mechanisms—the Néel mechanism associated with rotation of the magnetic moment within

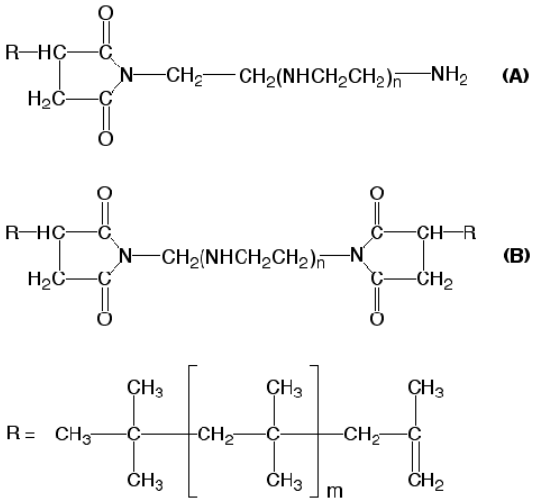

Figure 2. The structural formula of modified PIB ($m = 41, n = 4$). The substance used is 40–50% of a 1:1 mixture of the compounds A and B in a mineral oil.

the particle (relaxation time τ_N) and the Brownian relaxation by thermal rotation of particles in the solvent (relaxation time τ_B) [26]:

$$\tau_B = \frac{4\pi\eta a_h^3}{kT} \tag{18}$$

$$\tau_N = f_0 \exp\left(\frac{K\frac{4\pi}{3}a_M^3}{kT}\right) \tag{19}$$

with η the viscosity of the solvent, f_0 the Larmor frequency (about 10^9 s^{-1}) and K the material-dependent anisotropy constant. The characteristic relaxation time τ is given by [27]

$$\tau = 1/(1/\tau_N + 1/\tau_B). \tag{20}$$

When the only relaxation mechanism involved is Brownian rotation ($\tau_N \gg \tau_B$), the frequency ω_{max} at which χ'' reaches a maximum for monodisperse spherical particles with hydrodynamic radius a_h is [27]

$$\omega_{max} = kT/4\pi\eta a_h^3. \tag{21}$$

3. Experimental details

3.1. Materials and methods

Iron pentacarbonyl (Fluka Chemika) was taken from new bottles. Decalin (Merck), oleic acid (Merck, extra pure) and modified polyisobutene (PIB) coded SAP 285, consisting of a mixture of two polymers (figure 2) in a mineral base oil (Shell Research Ltd, UK), were used as supplied. The modification of PIB is reported elsewhere [28]. According to the supplier, the molecular weight of the PIB is 2400 g mol^{-1} and the polyisobutene/polyamine ratio is 2.0–2.5. To protect the iron particles against oxidation, all dispersions were always treated and stored under dried nitrogen atmosphere, using a glove box with oxygen pressure lower than 12 ppm as measured by an M Braun MB-OX-SE1 active oxygen probe.

Table 1. Amounts of reactants used for synthesis of iron dispersions.

Dispersion code	$Fe(CO)_5$ (ml)	SAP 285 (g)	Oleic acid (g)	Decalin (ml)
A	5	17.5	—	420
B	41	17.5	—	420
C	70	17.5	—	420
D	70 + 56	17.5	—	420
E	70 + 134	17.5	—	420
OA	44	—	4	20

3.2. Synthesis of iron and magnetite dispersions

Dispersions of oleic-acid-coated magnetite (Fe_3O_4) particles in toluene were synthesized by coprecipitation of Fe^{2+} and Fe^{3+} salts following [29] and coded FFOl. Dispersions of monodisperse iron particles were synthesized by thermal decomposition of iron pentacarbonyl in decalin, in the presence of a stabilizing surfactant (PIB or oleic acid) following [18]. After addition of $Fe(CO)_5$ to a solution of SAP 285 in decalin, the mechanically stirred solution was refluxed under nitrogen atmosphere for 24 h at 170 °C, using an oil bath. The size of the colloidal particles was tuned by varying the $Fe(CO)_5$/surfactant ratio. The amounts of iron pentacarbonyl, decalin and surfactant used are presented in table 1.

Particles were synthesized with average radii in the range 2–10 nm. Dispersions of PIB-coated particles were coded A to E, alphabetically ordered with increasing size. To prepare particles with a large radius (dispersions D and E), extra iron pentacarbonyl was added to a dispersion of smaller particles (dispersion C) in portions of approximately 15 ml every few hours. Earlier experiments starting with a large amount of $Fe(CO)_5$ without seeds resulted in unstable dispersions. For this seeded growth the heating was stopped a few hours after the last portion had been added. Dispersions of oleic-acid-coated particles were coded OA.

3.3. Characterization of iron and magnetite dispersions

Using a Philips CM10H TEM, micrographs were made of particles retained on grids coated with a Formvar film. The grids were placed in the vacuum of the sample holder of the microscope within 3 min after the opening of a glove box under nitrogen atmosphere, in which grids were made by dipping them in a dilute dispersion and letting them dry. Grids of the dispersion FFOl were made in air. Particle size distributions were measured using IBAS, an interactive image analysis program. Small-angle x-ray scattering experiments were performed at the DUBBLE (the Dutch–Belgian beamline) at the ESRF (Grenoble). The wavelength was fixed at 0.124 nm. The measurements were performed on dispersions A to E and OA, sealed in round glass capillaries. The measured two-dimensional diffraction patterns were corrected for transmission, background radiation and detector response. All measured intensities are in arbitrary units and have only relative relevance. Particle radii were determined from the initial slope of Guinier curves of dilute samples, using equations (9) and (10). These values were corrected for polydispersity measured with TEM, using equation (11). Interparticle distances were determined from the structure factors of concentrated samples following equation (12).

Magnetization curves of dilute dispersions were measured at room temperature on an alternating gradient magnetometer (AGM) Micromag 2900 (Princeton Measurements Corporation) in small airtight glass cups, filled in a glove box (except for the dispersion FFOl). Curves were fitted by the Langevin equation (1), from which M_s was determined. χ_i was determined from the slope of the curves at low magnetic fields (<1000 A m^{-1}). Assuming a

spherical particle shape, particle radii were calculated via equation (3), using the bulk values for m_s (see table 2). The number of particles n in a sample was determined from M_s, which is equal to $n\mu$. Knowing the sample volume, the particle concentration could be determined. This small volume of samples for AGM measurements (approximately 3 μl) was accurately determined by scaling of χ_i with the susceptibility measured on much larger known volumes of the same dispersions, using a Kappabridge KLY-3 susceptibility meter (Agico). For dispersions A to E and OA, the content of iron was determined by elemental iron analysis of a known mass of dispersion from which the iron particles were extracted after flocculating them by addition of pentanol.

3.4. Cryo-TEM experiments

Most cryo-TEM work reported in the literature has been performed on aqueous samples [30], which are usually vitrified in liquid ethane. However, decalin and toluene were found to dissolve into ethane, making it impossible to produce glassy films in this way. We found that these solvents could readily be vitrified in liquid nitrogen, despite its lower cooling efficiency in comparison with liquid ethane [31]. Vitrified films were made from dispersions on grids coated with holey carbon film (R2/2, Quantifoil Micro Tools GmbH) using a Vitrobot [32] in an oxygen-poor atmosphere (approximately 0.4 vol% O_2) to prevent particle oxidation. After placing a droplet of the dispersion onto the grid, a Vitrobot automatically blotted the liquid with filter paper, producing a liquid film in the grid holes (diameter 2 μm) which was thin in the middle (of the order of a particle diameter) and thicker at the edges of the hole. Then the specimen was plunged into liquid nitrogen, which caused the solvent to glassify. In addition, samples C and D were vitrified in a magnetic field after blotting by hand of a grid that was fixed between the poles of a strong magnet (1.6 T). Vitrification was performed by plunging the grid, fixed between the magnet poles, into liquid nitrogen. In this case particles were exposed to air for a time short enough ($\sim$40 s) to prevent formation of any observable oxidized layers around particle cores, which we usually observed for particles exposed to air for a few hours. Keeping samples in liquid nitrogen, they were placed into a cryo-holder which was mounted and examined in a Philips CM12H electron microscope at $-170\,^{\circ}$C and 120 kV. Photographs were taken from thin parts in carbon film holes with a Philips CM12 TEM at 120 kV using low-dose techniques. For dispersion D, vitrification in a magnetic field resulted in a film that was extremely susceptible to electron beam radiation damage. The film stability was increased considerably by the addition of small particles A. For comparison, the same mixture has also been vitrified without a magnetic field, giving similar pictures to samples without particles A.

3.5. EELS measurements

Energy electron loss spectroscopy (EELS) [33] was performed on cryo-TEM grids of dispersions A and D on a Philips Tecnai 12 Biofilter TEM. The film thickness x of the vitrified films was determined by the relation between the intensity I_{un} of the zero-loss peak (corresponding to the electrons that do not interact with the vitrified film) and the total intensity I_0, given by [34]

$$I_{un} = I_0 \exp\left(\frac{-\rho x}{(\rho x)_c}\right) \tag{22}$$

where $(\rho x)_c$ is the critical mass thickness (100 ± 10 nm g ml^{-1} for most solvents [34]) and ρ the density of the vitrified film (estimated as 0.9 g ml^{-1} for decalin).

3.6. Image analysis

Cryogenic electron micrographs were analysed, using an image analysis program (AnalySIS). Because the particle concentration in a cryo-film cannot be controlled very well experimentally and usually varies on different parts of the grid, the final concentration was determined by measuring the area that is occupied by iron cores on the micrographs. Division of this area by the total micrograph area results in a surface fraction of particles ϕ_s. The radial distribution function $g(r)$ of particle positions was calculated using special software (IDL). Cluster sizes were determined by dilation of particles using IBAS, an interactive image analysis program. Particles were considered part of the same cluster when the shortest distance between particle edges was not larger than the mean core radius.

3.7. Susceptibility measurements

For all iron dispersions, susceptibility measurements were performed in a large frequency range (1–100 000 Hz) on a home-built susceptibility meter (similar to the sensing coil described in [35]) that measures the local susceptibility at a chosen height of a sample tube. The set-up consists of two concentric coils, one (the primary coil) connected to an AC supply and the other (secondary coil) to a lock-in amplifier as the AC voltmeter. Samples were made in long glass tubes under nitrogen atmosphere. The susceptibility was determined from $V(\omega)$, which was measured while a sample was positioned in the coils, using equation (15). The signal of a reference sample (solvent) was subtracted from the signal of the ferrofluid. To check the stability of the dispersions, susceptibility measurements at a low frequency were performed as a function of height on all iron dispersions using the same set-up.

4. Results and discussion

4.1. Synthesis and characterization of ferrofluids

Approximately 30 min after starting the synthesis of iron dispersions the yellow iron pentacarbonyl solution turns either brown (dispersion A) or black (for larger particles), due to formation of iron. Particles with different average radii in the size range 2–10 nm with a polydispersity of 7–18% can be synthesized. The particles do not consist of pure iron, but also contain carbon. From Mössbauer spectroscopy measurements on dispersions C and E described and discussed elsewhere [36], the particle composition is concluded to be $Fe_{0.75}C_{0.25}$. The same composition was also found by other authors [37] for oleic-acid-coated iron particles synthesized via the same method as we used. Therefore, it is a plausible assumption that particle cores in all iron dispersions described in this paper consist of $Fe_{0.75}C_{0.25}$. Characterization results of all dispersions are summarized in table 2.

Sizes measured with different techniques correspond reasonably well with each other (table 2). However, radii measured with TEM presumably contain a relatively large uncertainty, since we found that radii measured on various electron microscopes differed by up to 20%. Particle radii determined from magnetization measurements are smaller than TEM radii, presumably because a non-magnetic layer is always present at magnetic particle surfaces and, moreover, we used the bulk value for m_s, which may not be the same for small particles. Since the interaction potential is very sensitive to particle size, the spread in particle radii in table 2 only allows a qualitative estimate of this potential. For dispersion E, magnetization curves could not be fitted with the Langevin function, due to hysteresis effects. As will be discussed later, a plausible reason for this behaviour is the presence of larger particle structures in the dispersion. From the interparticle spacing derived from the positions of the maximum

Table 2. Characterization of iron and magnetite dispersions.

Code	a_{TEM}[a] (nm)	a_{SAXS}[b] (nm) (a_{CORR}[c]) (nm)	a_M[d] (nm)	μ_{AGM}[e] ($\times 10^{19}$ A m^2)	Fe amount (mass fraction)[f]	Concentration (particles l^{-1})[g]
A	2.1 ± 0.3	2.17 (1.92)	1.3	0.123	0.004	1.7×10^{19}
B	6.0 ± 0.7	4.88 (4.44)	4.1	4.149	0.038	5.1×10^{18}
C	6.6 ± 1.1	6.03 (5.11)	5.1	8.38	0.061	8.2×10^{18}
D	6.9 ± 1.0	8.82 (7.76)	6.0	13.19	0.108	—
E	8.2 ± 1.5	9.54 (8.02)	—	—	0.219	—
OA	4.3 ± 0.3	3.87 (3.75)	3.3	2.29	0.257	1.4×10^{20}
FFOl	5.5 ± 2.5	—	5.1	3.24	—	—

[a] Particle radius measured from TEM micrographs.
[b] Particle radius determined from Guinier curves using equations (9) and (10).
[c] Guinier radius corrected for polydispersity (from TEM) using equation (11).
[d] Magnetic radius determined from magnetization curves (equation (3)).
[e] Dipole moment $\mu = 4\pi a_M^3 m_s/3$ with bulk value for $Fe_{0.75}C_{0.25}$ ($m_s = 1.49 \times 10^6$ A m^{-1} [38]) or Fe_3O_4 (0.48×10^6 A m^{-1} [16]).
[f] Amount of iron in dispersion from elemental analysis (g of Fe/g dispersion).
[g] Determined from magnetization measurements. This concentration could not be determined for dispersions D and E, since the susceptibility (necessary for calibration of the sample volume), is frequency-dependent in the range of operating frequencies of the magnetometer.

in the static structure factor of SAXS scattering curves of dispersion C, a thickness of the polymer layer of 7.0 ± 0.4 nm was determined. Susceptibility measurements show that particles oxidize fast (timescale of minutes) to a non-magnetic oxide on exposure of dispersions to air. Susceptibility measurements as a function of height confirm that all dispersions in this study, which were always kept under nitrogen, are stable and do not phase separate.

4.2. Cryo-TEM experiments

In aqueous samples, film stability is based on a balance of attractive van der Waals forces between the air–liquid interfaces and electrostatic repulsions between charged surfactants organized at these interfaces [39]. Making stable glassy films of organic solvents is not trivial [30] and only a few reports have appeared [40]. We found that thin films of ferrofluids in organic solvents are surprisingly stable, despite the absence of charged surfactants, and that they could readily be vitrified in liquid nitrogen. Film thicknesses determined from EELS measurements varied considerably for different parts of the grid, but were of the order of a particle diameter. An illustrative example of variation of film thickness in a grid hole is shown in figure 3, where the thickness increases from the hole centre (lower right corner), with only one layer of individual particles, to the edge of the grid hole (upper left corner), where particles are arranged into linear chains due to the high concentration and presumably are positioned in different layers.

4.2.1. Influence of particle size. Figure 4 shows typical examples of cryo-TEM micrographs of a dilute ferrofluid of oleic-acid-coated magnetite particles in toluene (FFOl), where clusters of colloids are present with an isotropic shape, most probably caused by van der Waals attractions and weak magnetic attractions, which are both of the order of kT. Note that

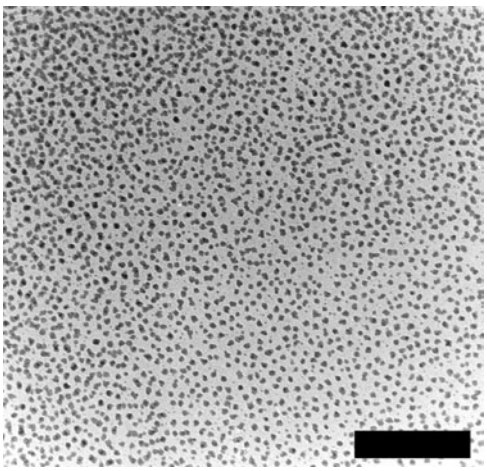

Figure 3. An example of a cryogenic electron micrograph of dispersion B with gradually increasing film thickness going from the lower right corner to the upper left corner. Aggregate sizes increase with concentration (see the text). The scale bar corresponds to 200 nm.

these micrographs are snapshots of the ferrofluid; since all dispersions described in this paper are stable (as found from sedimentation experiments and susceptibility measurements as a function of height), cluster formation is presumably reversible or permanent aggregates are small enough to sediment very slowly. Figure 5 shows cryo-TEM micrographs of dispersions A to E (i.e. dispersions of PIB-coated iron particles for increasing particle size). In contrast to the magnetite dispersions, where dipolar interactions appear to be too weak to form linear aggregates, in iron ferrofluids we clearly observe linear structures at zero field (figure 5(d)) as predicted by de Gennes and Pincus [2]. These randomly organized chains very much resemble the fluctuating chains found in simulations of dipolar fluids [3, 4, 11]; see figure 6. As confirmed by simulations [7, 11], chains do not aggregate to larger clusters, showing that chain–chain interactions are weak. The presence of many individual particles in figure 5(d) indicates that chains are dynamic and easily disrupted due to thermal motion. Despite the large number of single particles, the mean number of particles per cluster is 2.49 due to the presence of many larger clusters (see figure 7 for a histogram). However, for larger particles (figure 5(e)), cluster sizes increase considerably and almost no single particles are found, obviously an effect of much stronger dipole–dipole interactions. Smaller particles, magnetically interacting more weakly, show an ordered configuration (see figures 5(b), (c)), where particles stay separated, because isotropic steric repulsion between their thick surfactant layers is the dominant interaction. This is in contrast to the case for oleic-acid-coated magnetite particles, where van der Waals interactions cannot be neglected and isotropic clusters are present. For the ordered structure of dispersion B the particle concentration is so high that we expect the interparticle distance to be of the order of two particle surfactant layers t_s. Assuming this, t_s can be estimated from the average centre–centre distance between nearest-neighbour particles (which is determined as 24.8 ± 2.5 nm) by subtraction of the TEM core diameter (12.0 nm) and dividing by 2, giving a value of $t_s = 6.4$ nm, which corresponds very well with 7 nm, found from the first peak of the structure factor as measured by SAXS. These values are in agreement with the expected maximum thickness of the PIB layer of 7–8 nm, assuming C–C bond lengths of 0.154 nm and bond angles of 110°. Note that for dispersions D and E, particles within a cluster are much closer than would be expected from the thickness of the PIB layer; for example, the distance

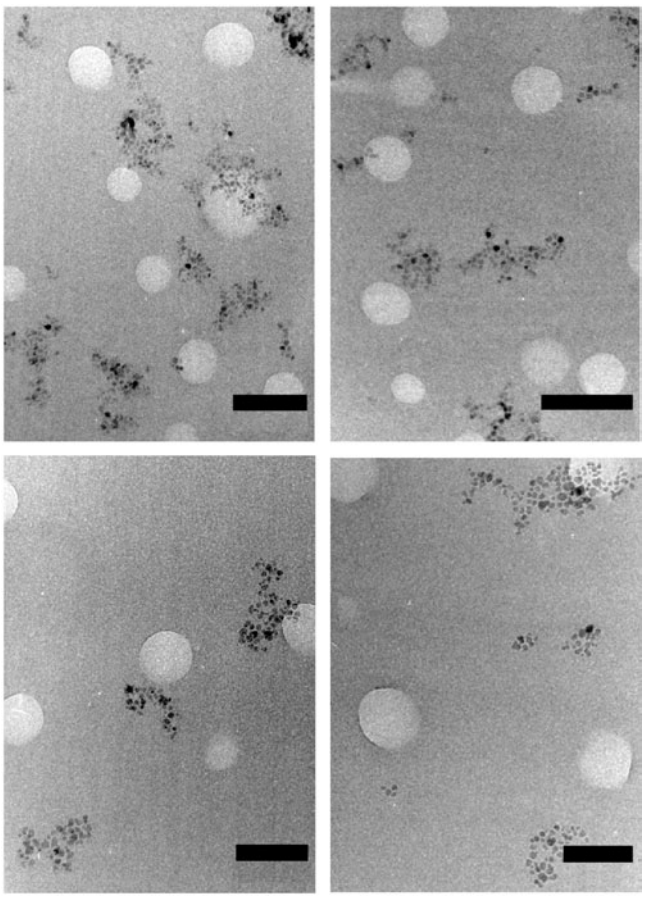

Figure 4. Typical cryogenic electron micrographs of a dispersion of magnetite particles in toluene (FFOl) glassified in liquid nitrogen. The scale bar corresponds to 200 nm. The large white objects are artefacts.

between core edges of close particles in dispersion D are of the order of 3–4 nm. Here, dipolar interactions are large enough to compress the polymer layers. In addition, the surfactant layers of particles D and E might be somewhat thinner because the grafting density of PIB is lower (and therefore the polymer chains are less extended) in comparison with that of smaller PIB-coated particles, due to the different method of synthesis (particles D and E are grown from seed particles C without adding extra PIB). From figure 5 it is clear that the particle structure in ferrofluids is very sensitive to particle size, as expected from the scaling of dipolar interactions with a_M^6/σ^3 for particles at contact (equation (5)). It must be noted however, that cryo-TEM images thin films of dispersions (thickness of the order of one particle diameter), which ought to be considered as two-dimensional. Nevertheless, the presence of anisotropic structures is not limited to thin films; as will be discussed later, susceptibility measurements on the same dispersions show that larger structures are also present in three-dimensional ferrofluids.

Dried samples, required for conventional TEM, show significantly different ordering of particles in comparison with cryo-TEM of vitrified films of dispersions, as can be seen in figure 8, where some TEM micrographs are presented. While cryo-TEM micrographs are reproducible for a given dispersion, conventional TEM pictures show large differences between

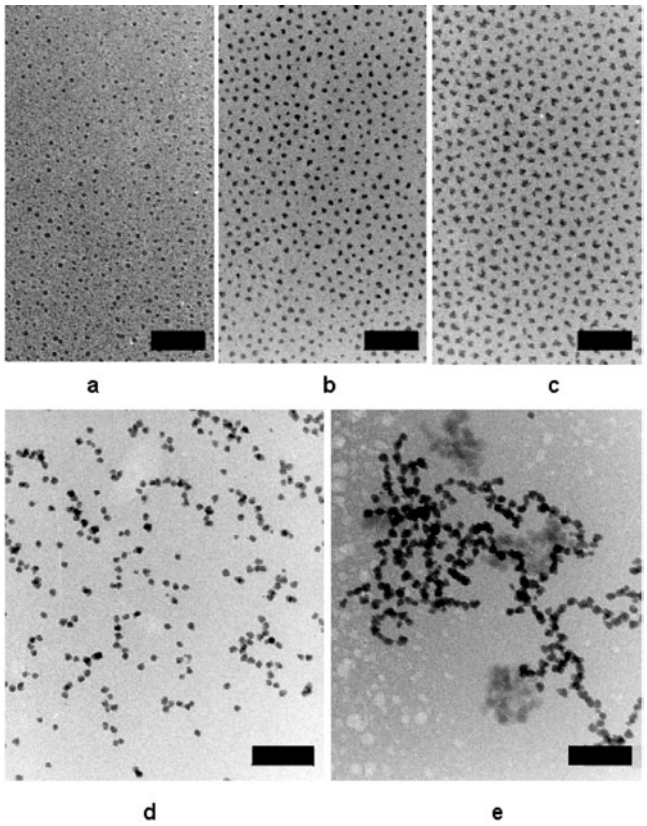

Figure 5. Typical cryogenic electron micrographs of dispersions of PIB-coated iron dispersions with increasing average particle radius, determined from separate TEM measurements. (a) 2.1 nm (referred to as particles A); (b) 6.0 nm (particles B); (c) 6.6 nm (particles C); (d) 6.9 nm (particles D); (e) 8.2 nm (particles E). The scaling bars correspond to 100 nm. In (e), the white patches on the left and the three larger structures with poor contrast are artefacts.

various pictures of the same dispersion (compare figures 8(a) and (b)). In addition, drying of grids clearly induces cluster formation, as the clusters in figure 8 are much larger than in the same dispersions in figure 5.

4.2.2. Influence of surfactant layer. We studied two dispersions with comparable iron core sizes, but different thicknesses of their surfactant layers (dispersion OA ($a_{TEM} = 4.3$ nm, coated with oleic acid) and dispersion B ($a_{TEM} = 6.0$ nm, PIB coated)), to investigate the effect of the range of steric repulsion between particles. The dipole–dipole interactions between two particles in a head-to-tail configuration at minimum distance (i.e. including the core diameter and two surfactant layers) can be calculated using equation (5) with the experimental value for μ from table 1 and $r = 2(a_{core}+t_s)$. However, values for particle sizes measured with different techniques are not equal and consequently give different interaction energies. The thickness of the oleic acid layer was not determined, but a thickness of 1–2 nm is usually assumed. Using different values for r, U_{max} ranges from 0.48 kT ($a_{core} = 6.0$ nm, $t_s = 7.0$ nm) to 1.39 kT ($a_{core} = 4.4$ nm, $t_s = 4.7$ nm) and from 1.3 kT ($a_{core} = 4.3$ nm, $t_s = 2.0$ nm) to 3.1 kT ($a_{core} = 3.7$ nm, $t_s = 1.0$ nm) for dispersions B and OA respectively. Despite the large spread

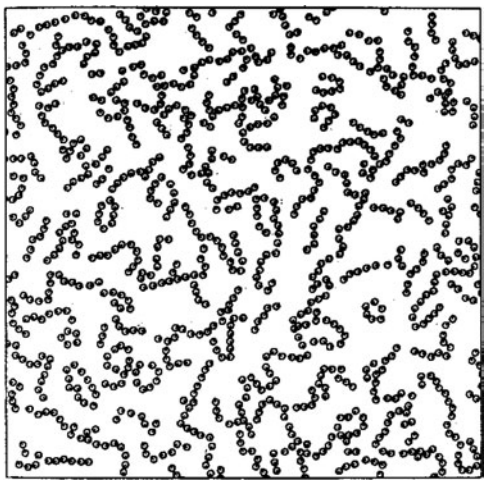

Figure 6. A snapshot of a two-dimensional Monte Carlo simulation of cobalt particles of 15 nm diameter with a surfactant layer of 2 nm (from Chantrell [4]).

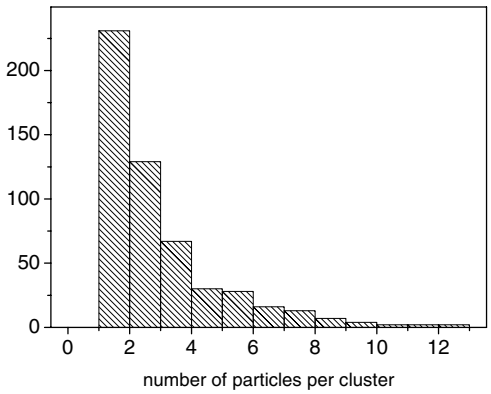

Figure 7. The distribution of cluster size, as determined from different cryo-TEM micrographs of dispersion D. Particles were assumed to be part of the same cluster if the surface-to-surface distance between neighbouring particles was smaller than the mean particle radius. The mean number of particles per cluster is 2.49.

in U_{max}, these values show that due to the smaller surfactant layer, dipole–dipole interactions are larger for particles OA than for particles B. Typical examples of the two dispersions for a comparable surface fraction of iron cores ($\phi_s = 0.14$ and 0.13 respectively) are shown in figures 9(a) and (b), which are indeed different. Although particles from dispersion OA seem to form loose linear structures, we are not sure whether they are resulting from dipolar interactions, since particle distances are rather large. In contrast, figure 9(b) (dispersion B) shows separate particles with strong ordering. The corresponding radial distribution functions of the particle positions from figures 9(a) (dispersion OA) and (b) (dispersion B) are also presented in figure 9. While for dispersion OA $g(r)$ is approximately 1 for all values of r (no order), for dispersion B at least two clear peaks are seen, indicating an ordered structure with dominant interparticle distances of 25.2 and 49 nm (corresponding to the peak maxima). Presumably in figure 9(b) the surface fraction of particles (including cores and thick surfactant

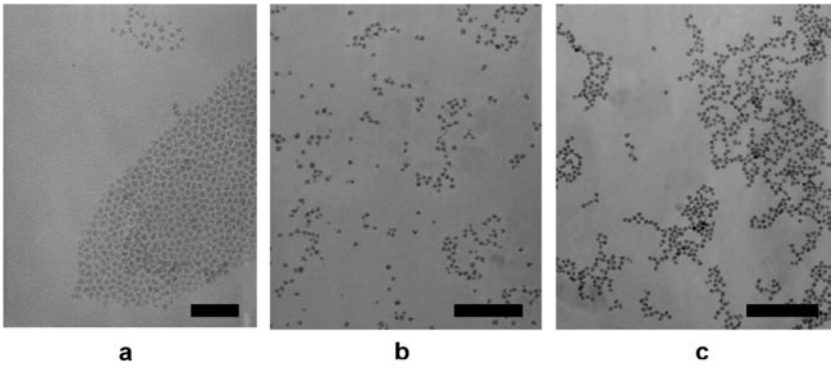

Figure 8. Conventional TEM pictures of dried samples of ((a), (b)) dispersion C, (c) dispersion D. The scale bars correspond to 100 nm (a) and 200 nm ((b), (c)). Particle structures are significantly different from structures in cryo-TEM micrographs of the same dispersions (compare with figures 5(c), (d)) and not reproducible (compare figures 8(a), (b)).

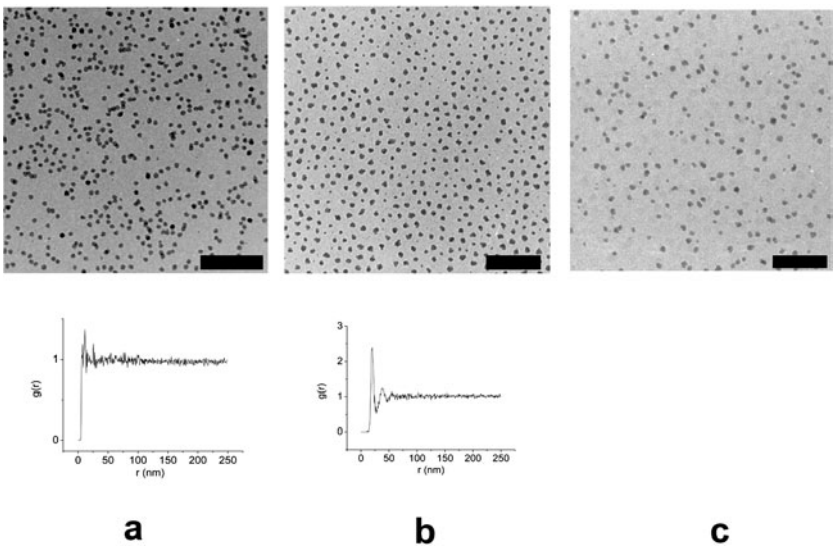

Figure 9. Examples of cryogenic electron micrographs of dispersions of iron particles coated with different surfactants, glassified in liquid nitrogen. (a) Dispersion OA (oleic acid coated, a_{core}(TEM) = 4.9 nm, $\phi_s = 0.14$); (b) dispersion B (PIB coated, a_{core}(TEM) = 6.0 nm, $\phi_s = 0.13$); (c) dispersion B ($\phi_s = 0.05$). The scale bars correspond to 100 nm.

layers) is so large that steric repulsion forces are dominant and no chain formation can occur because particles are too tightly packed. However, for lower concentrations of particles B also (figure 9(c)), no clear chain formation is found, indicating that dipolar interactions are indeed rather small. Although dipolar attractions are calculated to be higher for dispersion OA, and cryo-TEM micrographs show a clear difference from dispersion B, the interactions seem to be too small to result in the presence of very distinct linear chains, such as are seen for dispersion D (figure 5(d)).

4.2.3. Influence of particle material. Although for dispersions OA (figure 9(a)) and FFOl (figure 4) the dipolar interactions are estimated to be in the same range (1.3–3.1 kT and 1.5–2.8 kT (for ($a_{core} = 5.5$ nm, $t_s = 2.0$ nm) and ($a_{core} = 5.1$ nm, $t_s = 1.0$ nm) respectively), there is a large difference in particle structure between clearly isotropic clusters for magnetite particles and the presence of only a few anisotropic clusters which seem to be induced by dipolar interactions for dispersion OA. It must be noted that an accurate estimate of particle interactions is very hard for small magnetic colloids with thin surfactant layers; in particular, the van der Waals interaction is extremely sensitive to interparticle distance, resulting in a large uncertainty in the interaction potential. That the polydispersity (which is found to enhance aggregation [41]) and particle shape differ in the two dispersions makes quantitative predictions even more complicated. However, the cryo-TEM results show that dominant interactions in the magnetite dispersion FFOl are clearly isotropic (van der Waals) attractions, whereas they probably are dipolar in the iron dispersion OA.

4.2.4. Influence of magnetic field. If the linear structures as found in dispersion D (figure 5(d)) are due to dominating dipolar attractions, they should align in a magnetic field. Indeed, figure 10 shows that the randomly oriented chains that exist in zero field (figure 10(a)), are all aligned in the direction of the saturating magnetic field (1.6 T; figure 10(b)). Aggregates are much longer, presumably because orientation of all dipoles in one direction increases the mean dipole–dipole attraction between particles or particle chains. In addition, shape fluctuations in parallel chains give rise to chain–chain interaction perpendicular to the field direction, causing the formation of thick sheets of particles due to lateral aggregation. It is observed that films of particles D are stable without a magnetic field but only marginally stable with a large magnetic field, which suggests that the presence of homogeneously distributed particles is necessary to stabilize the films. When big clusters of particles D are formed, leaving large areas without any particles, the addition of the much less magnetic particles A leads to stabilization by ensuring that particles remain distributed throughout the film. Aggregates similar to those in figure 10(b) are found in magnetorheological and electrorheological fluids [42, 43] and dispersions of non-magnetic particles in ferrofluids [44, 45]. These cases, however, involve induced dipoles that lose their magnetic moments on turning off the magnetic field, whereas in our dispersions permanent dipoles already form linear aggregates in zero field. It appears also that individual particles that magnetically interact too weakly to form clusters (dispersion C) do respond to high magnetic fields. Because our iron particles are not completely spherical, their magnetic moments may be preferentially oriented along the longer particle axis, due to magnetic shape anisotropy. Indeed, upon application of a saturating magnetic field ($\mu_0 \mu H / kT \approx 328$; figure 10(d)), the C particles orient in the direction of the magnetic field, resulting in an image where longer particle axes mostly point in the same direction (see the histograms in figures 10(c), (d)). Although in this case magnetic interparticle interactions will be larger than in zero field, they remain too weak to cause magnetic field-induced aggregation.

4.2.5. Susceptibility measurements. The frequency-dependent susceptibility curves for dispersions B, C, D and E are presented in figure 11. For dispersion A, the susceptibility was too low to be measured accurately. For dispersions B and C in figures 11(a) and (b) respectively, a maximum in the susceptibility (equation (21)) is expected at a frequency corresponding to single-particle rotation (31 and 24 kHz for a hydrodynamic particle radius a_h of 11.9 nm ($a_{core} = 4.9, t_s = 7.0$) and 13 nm ($a_{core} = 6.0, t_s = 7.0$) respectively). For particles B, the susceptibility maximum is at a higher frequency than the measuring range, presumably because the dipole moments rotate inside the particles (Néel relaxation). For particles C, the

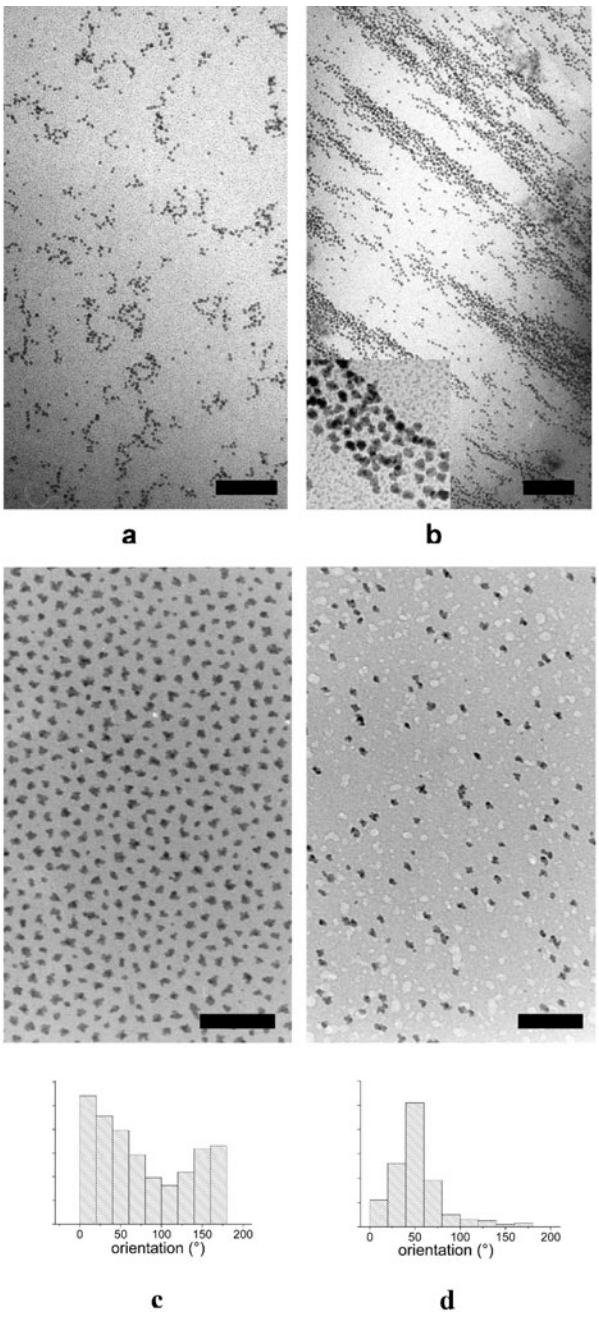

Figure 10. Examples of cryogenic electron micrographs made from dispersions D (mixed with dispersions A, with iron volume fractions of particles D and particles A of 0.0006 and 0.0004 respectively) and dispersions C. (a) Dispersion D in zero field. (b) Dispersion D in a saturating magnetic field. The inset is an enlargement (2.5 times) of a part of the complete picture. The scaling bars correspond to 200 nm. Chains, already existing in zero field, align in the magnetic field. (c) Dispersion C in zero field. (d) Dispersion C in a saturating magnetic field. The scaling bars correspond to 100 nm. Individual particles align in the field direction. Histograms presenting the orientation distribution of the longest particle axes show that particles C are oriented randomly in zero field, while the orientation is peaked in a saturating magnetic field.

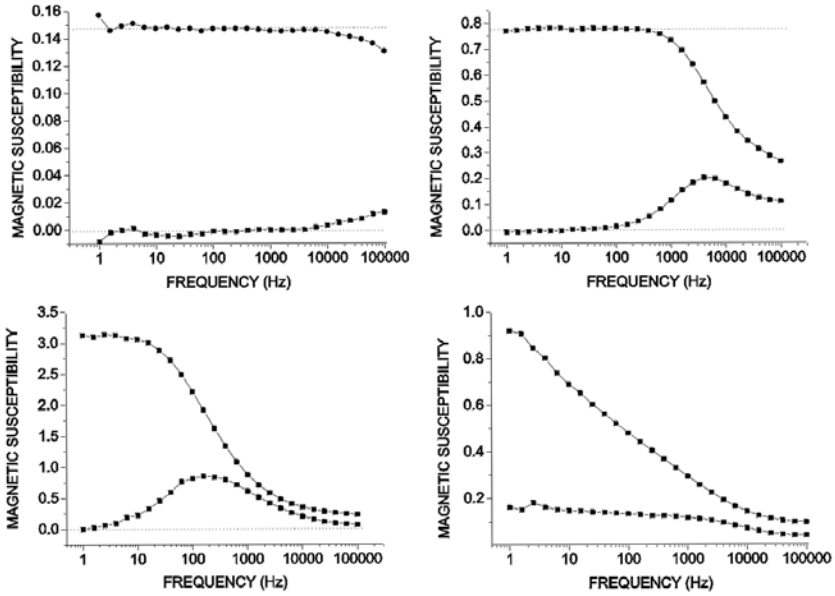

Figure 11. Curves of the real (upper curve) and imaginary susceptibility (lower curve) as a function of frequency. (a) Dispersion B; (b) dispersion C; (c) dispersion D; (d) dispersion E.

maximum found is of the order of magnitude of the theoretical value, although somewhat lower than expected (4000 Hz), probably because these particles are not completely spherical (see figure 5(c)), which will increase the Brownian rotation time. However, for particles D (figure 11(c)), a maximum in the susceptibility is found at approximately 150 Hz, much lower than expected for single particles. For dispersion E (figure 11(d)) a maximum is not even reached at a frequency of 1 Hz. These results clearly indicate that much larger structures must be present in dispersions D and E, in agreement with what was found from cryo-TEM. Most probably, this is also the reason for hysteresis in the magnetization curves of dispersion E, because the lower-frequency limit of the AGM is 100 Hz, which is too high for relaxation of the large particle structures present. For dispersion OA, where the susceptibility maximum for single Brownian particles is expected at 208 kHz (and the onset of the imaginary susceptibility at a lower frequency), no imaginary contribution is found. Probably, these particles perform Néel relaxation. The absence of an imaginary susceptibility confirms that these particles interact only very weakly; the structures seen on cryo-micrographs for these dispersions, indeed looking very loose in contrast to those for dispersions D and E, are reversible on a timescale of the measuring frequency (up to 100 kHz). Although we cannot give a decisive answer about the exact particle morphologies, we conclude that cryo-TEM presents at least a quantitative correct picture for fluids in three dimensions.

4.2.6. Comparison with theory and simulations. As in many simulations [3, 4, 7], we do not find signs of phase separation in our ferrofluids. However, supporting several theories and simulations [2, 7, 9, 11], our results experimentally demonstrate the presence of linear structures in ferrofluids in zero field for large enough dipoles. Our results qualitatively agree with simulations in two and three dimensions, where fluctuating chains are found that thermally dissociate and recombine again. Although in some simulations ring-like structures are found [46], we did not see any in our samples. Almost no quantitative results are known

for simulations on ferrofluids in two dimensions, but our results can be compared to theories and simulations in three dimensions. Here, the onset of chain formation roughly starts at a dimensionless reduced dipole moment μ^* (defined as $(\mu_0\mu^2/4\pi kT\sigma^3)^{1/2}$ with μ_0 the permeability of free space and σ the hard-sphere diameter) of 2–2.5 with an average chain length varying from 1.36 to 10.25 particles for a concentration ρ^* (defined as $N\sigma^3/V$ with N/V the number of particles per volume) of 0.3 [7]. This value is similar to our experimental results, where for iron particles in dispersion D, chain formation starts with a value of 2.4 for μ^* (with $\mu = 13.2 \times 10^{-19}$ A m^2 and $\sigma = 25$ nm ($a_{core} = 6.9$ nm, $t_s = 6$ nm)) and a mean cluster size of 2.49 for a 'two-dimensional' concentration ρ_s^* (defined as $N\sigma^2/A$ with N/A the number of particles per unit of surface) of 0.4.

5. Conclusions

We have exploited the possibility of synthesizing dispersions of monodisperse iron particles by thermal decomposition of $Fe(CO)_5$, for which the size and the type of polymeric stabilization layer can be controlled. Larger particles can be grown from seed particles by adding extra $Fe(CO)_5$. We have shown that cryo-TEM is a valuable technique for studying (magnetic) dispersions: particles can be directly imaged *in situ*, giving a realistic view of how particles are organized in a liquid film of the dispersion. Frequency-dependent susceptibility measurements indicate that particle structures in zero field in three-dimensional ferrofluids resemble those in liquid films.

Our experiments for the first time directly visualize the presence of linear clusters in ferrofluids in zero field. Ferrofluid structures appear to be very sensitive to particle size; upon systematically increasing particle size, we find an abrupt transition from separate particles to randomly oriented linear aggregates and even branched networks. These results qualitatively agree with simulation results [3, 4, 11]. The linear structures we find are indeed dipolar, as is confirmed by their response to high magnetic fields; existing chains at zero field align and grow larger in the field direction as well as perpendicular to that due to lateral attraction. Individual non-aggregated iron particles appear to be magnetically anisotropic due to their particle shape, and align their dipoles with a magnetic field.

For oleic-acid-coated particles a quantitative estimate of interactions between particles is difficult due to their thin surfactant layer, and van der Waals interactions cannot be ignored. However, PIB-coated iron particles, where the polymer layer masks the van der Waals attraction and dipolar interactions are adjustable, may well be the experimental equivalent of dipolar spheres in computer simulations [7].

Acknowledgments

Dispersion FFOl was synthesized by Dr Bica (University Politechnica in Timisoara, Romania). Liesbeth Donselaar is thanked for assistance with cryo-TEM on the magnetite dispersions. Marc Storms and Felix de Haas from the FEI company are thanked for performing the EELS measurements. The autocorrelation functions were calculated by Roel Dullens. Maarten Terlou is thanked for his help with the image analysis and Ben Erné and Thido Arts for their help with the susceptibility measurements. Financial support was granted by the Dutch Technology Foundation (STW) with financial aid from the Council for Chemical Science of the Netherlands Organization for Scientific Research (CW/NWO).

References

[1] Butter K, Bomans P H, Frederik P M, Vroege G J and Philipse A P 2003 *Nature Mater.* **2** 88
[2] de Gennes P G and Pincus P A 1970 *Phys. Kondens. Mater.* **11** 189
[3] Weis J J 1998 *Mol. Phys.* **93** 361
[4] Chantrell R W, Bradbury A, Popplewell J and Charles S W 1982 *J. Appl. Phys.* **53** 2742
[5] Berkovski B and Bashtovoy V 1996 *Magnetic Fluids and Applications Handbook* (New York: Begel House)
[6] Lubbe A S, Alexiou C and Bergemann C 2001 *J. Surg. Res.* **95** 200
[7] Teixeira P I C, Tavares J M and Telo da Gama M M 2000 *J. Phys.: Condens. Matter* **12** R411
[8] Cabuil V 2000 *Curr. Opin. Colloid Interface Sci.* **5** 44
[9] Osipov M A, Teixeira P I C and Telo da Gama M M 1996 *Phys. Rev.* E **54** 2597
[10] Tlusty T and Safran S A 2000 *Science* **290** 1328
[11] Tavares J M, Weis J J and Telo da Gama M M 1999 *Phys. Rev.* E **59** 4388
[12] Shen L, Stachowiak A, Fateen S K, Laibinis P E and Hatton T A 2001 *Langmuir* **17** 288
[13] Donselaar L N, Frederik P M, Bomans P H, Buining P A, Humbel B M and Philipse A P 1999 *J. Magn. Magn. Mater.* **201** 58
[14] Cebula D J, Charles S W and Popplewell J 1983 *J. Physique* **44**
[15] Gazeau F, Dubois E, Bacri J C, Boue F, Cebers A and Perzynski R 2002 *Phys. Rev.* E **65** 031403
[16] Rosensweig R E 1985 *Ferrohydrodynamics* (Cambridge: Cambridge University Press)
[17] Griffiths C H, O'Horo M P and Smith T W 1979 *J. Appl. Phys.* **50** 7108
[18] Pathmamanoharan C, Zuiverloon N L and Philipse A P 2000 *Prog. Colloid Polym. Sci.* **115** 141
[19] Scholten P C 1992 *Studies of Magnetic Properties of Fine Particles and their Relevance to Materials Science* ed J L Dormann and D Fiorani (Amsterdam: Elsevier)
[20] Lavender H B, Iyer K A and Singer S J 1994 *J. Chem. Phys.* **101** 7856
[21] Philipse A P and Maas D 2002 *Langmuir* **18** 9977
[22] Halsey T C and Toor W 1990 *J. Stat. Phys.* **61** 1257
[23] Toor W R 1993 *J. Colloid Interface Sci.* **156** 335
[24] Dhont J K G 1996 *An Introduction to Dynamics of Colloids* (Amsterdam: Elsevier) ch 3
[25] Jiles D 1995 *Introduction to Magnetism and Magnetic Materials* (London: Chapman and Hall)
[26] Charles S W 1988 *Chem. Eng. Commun.* **67** 145
[27] Fannin P C, Scaife B K P and Charles S W 1986 *J. Phys. E: Sci. Instrum.* **19** 238
[28] De Hek B and Vrij A 1981 *J. Colloid Interface Sci.* **79**
[29] Bica D 1995 *Rom. Rep. Phys.* **47** 256
[30] Talmon Y 1996 *Ber. Bunsenges. Phys. Chem.* **100** 364
[31] Steinbrecht R A and Zierold K 1987 *Cryo Techniques in Biological Electron Microscopy* (Berlin: Springer)
[32] Frederik P M, Bomans P H H, Laeven P F J and Nijpels F J T 2002 Device for preparing specimens for a cryo-electron microscope *Netherlands Industrial Property Office (RO/NL)*
[33] Reimer L 1989 *Transmission Electron Microscopy: Physics of Image Formation and Microanalysis* 2nd edn (Heidelberg: Springer)
[34] Carlemalm E, Colliex C and Kellenberger E 1985 *Adv. Electron. Electron Phys.* **63** 269
[35] van Ewijk G A, Vroege G J and Kuipers B W M 2002 *Langmuir* **18** 382
[36] Goossens A, de Jongh L J, Butter K, Philipse A P, Craje M W J and van der Kraan A M 2002 *Hyperfine Interact.* **141** 381
[37] Hanson M, Johansson C, Pedersen M S and Morup S 1995 *J. Phys.: Condens. Matter* **7** 9269
[38] Bauer-Grosse E and Le Caër G 1987 *Phil. Mag.* B **56** 485
[39] Frederik P M, Stuart M C A, Schrijvers A H G J and Bomans P H H 1989 *Scanning Microsc.* 277
[40] Oostergetel G T, Esselink F J and Hadziioannou G 1995 *Langmuir* **11** 3721
[41] Bradbury A, Menear S and Chantrell R W 1986 *J. Magn. Magn. Mater.* **54–57** 745
[42] Gast A P and Zukoski C F 1989 *Adv. Colloid Interface Sci.* **30** 153
[43] Halsey T C 1992 *Science* **258** 761
[44] Skjeltorp A T 1983 *Phys. Rev. Lett.* **51** 2306
[45] de Gans B J, Blom C, Philipse A P and Mellema J 1999 *Phys. Rev.* E **60** 4518
[46] Tavares J M, Weis J J and Telo da Gama M M 2002 *Phys. Rev.* E **65** 061201